Title: The *Phtheirospermum japonicum* isopentenyltransferase PjIPT1a regulates host cytokinin responses in *Arabidopsis*

Authors: Anne Greifenhagen[1], Isabell Braunstein[1], Jens Pfannstiel[2], Satoko Yoshida[3], Ken Shirasu[4,5], Andreas Schaller[1], Thomas Spallek[1*]

Affiliations: [1]Department of Plant Physiology and Biochemistry, University of Hohenheim, Stuttgart, 70599, Germany

[2]Core Facility Hohenheim, Mass Spectrometry Unit, University of Hohenheim, Stuttgart, 70599, Germany

[3]Division of Biological Science, Graduate School of Science and Technology, Nara Institute of Science and Technology, Ikoma, Nara, 630-0192, Japan

[4]RIKEN Center for Sustainable Resource Science, Yokohama, 230-0045, Japan

[5]Graduate School of Science, The University of Tokyo, Tokyo, 113-0033, Japan

Corresponding Author: Thomas Spallek, address as above, Phone: +49 711-459-22200, email: thomas.spallek@uni-hohenheim.de

ORCID ID:

Anne Greifenhagen (Orcid ID: 0000-0003-2979-3203)

Isabell Braunstein (N/A)

Jens Pfannstiel (Orcid ID: 0000-0002-7651-4302)

Satoko Yoshida (Orcid ID: 0000-0002-9999-7861)

Ken Shirasu (Orcid ID: 0000-0002-0349-3870)

Andreas Schaller (Orcid ID: 0000-0001-6872-9576)

Thomas Spallek (Orcid ID: 0000-0003-4425-1015)

Total word count: 3141

4 main figures, 4 supplemental figures, 3 supplemental tables

Summary

The hemiparasitic plant *Phtheirospermum japonicum* is a nutritional specialist that supplements its nutrient requirements by parasitizing other plants through haustoria. During parasitism, the *Phtheirospermum* haustorium transfers hypertrophy-inducing cytokinins (CKs) to the infected host root. The CK biosynthesis genes required for haustorium-derived CKs and the induction of hypertrophy are still unknown. We searched for haustorium-expressed isopentenyltransferases (IPTs) that catalyse the first step of CK biosynthesis, confirmed the specific expression by *in vivo* imaging of a promoter-reporter, and further analysed the subcellular localization, the enzymatic function, and contribution to inducing hypertrophy by studying CRISPR-Cas9 induced *Phtheirospermum* mutants. *PjIPT1a* was expressed in intrusive cells of the haustorium close to the host vasculature. PjIPT1a and its closest homolog PjIPT1b located to the cytosol and showed isopentenyltransferases activity *in vitro* with differences in substrate specificity. Mutating *PjIPT1a* abolished parasite-induced CK responses in the host. A homolog of *PjIPT1a* with shared characteristics was also identified in the related weed *Striga hermonthica*. We propose that *PjIPT1a* exemplifies how parasitism-related functions evolve through gene duplications and neofunctionalization.

Keywords

Cytokinin, parasite, haustorium, intrusive cells, hypertrophy, *Striga*, neofunctionalization

Introduction

Most parasitic species maintain some level of photosynthesis (hemiparasites), but access soil nutrients mainly by parasitizing other plants (Heide-Jorgensen, 2008; Brundrett & Tedersoo, 2018). The two main lineages of hemiparasitic plants, Santalales and the family of Orobanchaceae in the Lamiales account for more than 90% of all parasitic species (Nickrent, 2020). The greatest in-family diversity of hemiparasitic plants is found in the Orobanchaceae. In contrast to the agriculturally important weed *Striga hermonthica*, non-weedy species such as the model parasitic plant *Phtheirospermum japonicum* can propagate without being attached to a host (Clarke *et al.*, 2019).

Genetic adaptations to the parasitic lifestyle start to be revealed from the sequencing of transcriptomes and genomes of parasitic plants (Yang *et al.*, 2015; Vogel *et al.*, 2018; Sun *et al.*, 2018; Yoshida *et al.*, 2019). At the centre of these studies is the haustorium, a multi-cellular organ that facilitates infection and parasitism (Yoshida *et al.*, 2016; Kokla & Melnyk, 2018). Comparative transcriptomics in three Orobanchaceae species with varying degrees of host dependencies unearthed remarkable conservation of the transcriptional signatures during infection (Yang *et al.*, 2015). Further studies confirmed these tendencies also in other lineages (Vogel *et al.*, 2018; Sun *et al.*, 2018; Yoshida *et al.*, 2019). The term “core parasitism genes” describes the shared transcriptional behaviour of a group of homologous genes within a parasitic plant lineage (Yang *et al.*, 2015).

The concept of core parasitism genes may be extended to “core parasitism strategies”. Strategies that are commonly observed during plant parasitism include the secretion of cell wall degrading enzymes and changes in hormone homeostasis (Brun *et al.*, 2020). For example, cytokinins (CKs) are produced in haustoria of *Cuscuta japonicum*, *Santalum album* and *Phtheirospermum japonicum* (Zhang *et al.*, 2012; Furuhashi *et al.*, 2013; Spallek *et al.*, 2017). Transfer of cytokinin from the parasite to the host was demonstrated using *Arabidopsis* cytokinin biosynthesis mutants and transgenic *Phtheirospermum* roots that express a cytokinin-degrading enzyme (Spallek *et al.*, 2017). With prolonged cytokinin transfer, infected host tissue becomes hypertrophic, a symptom that is also induced by mistletoes, *Viscum album* (Loranthaceae in the order Santalales), and *Alectra vogelii* (Orobanchaceae) (Heide-Jorgensen, 2008).

85 Cytokinins are N^6-substituted adenine derivatives, of which isoprenoid cytokinins are most
86 prevalent in plants (Sakakibara, 2006). N^6-prenylation is catalysed by adenosine phosphate-
87 isopentenyltransferases (IPTs, Fig. **1a**). Plant IPTs prefer dimethylallyl diphosphate (DMAPP)
88 as isoprenoid donor, and ATP and ADP (ATP/ADP-type IPTs) or tRNA (tRNA-type IPTs) as
89 isoprenoid acceptors (Kakimoto, 2001; Sakakibara, 2006). The agrobacterial IPTs, Tmr and
90 Tzs, prefer hydroxy-methylbutenyl diphosphate and AMP as substrates. Tmr and Tzs are
91 required for virulence and crown-gall formation (Akiyoshi *et al.*, 1984; Heinemeyer *et al.*,
92 1987). Overexpression of *IPT*s in *Arabidopsis* causes ectopic cytokinin responses (Kakimoto,
93 2001) indicating that IPTs catalyse the rate limiting step in cytokinin biosynthesis. In
94 *Arabidopsis*, the major route of cytokinin biosynthesis relies on ATP/ADP-type IPTs targeted
95 to plastids (AtIPT1, AtIPT3, AtIPT5, AtIPT8), to mitochondria (AtIPT7), or residing in the
96 cytosol and nucleus (AtIPT3, AtIPT4). tRNA-type IPTs (AtIPT2, AtIPT9) also localize to the
97 cytosol and nucleus (Kasahara *et al.*, 2004; Kieber & Schaller, 2014). The biological relevance
98 of different subcellular IPT locations is not known.
99
100 Here, we report the function of *Phtheirospermum* PjIPT1a as essential for triggering
101 *Phtheirospermum*-induced cytokinin responses in *Arabidopsis.* PjIPT1a is an unconventional
102 plant isopentenyltransferase with parasitism-related features. PjIPT1a uses AMP and ATP as
103 prenyl acceptors and is located in the cytosol. It is expressed in intrusive cells of the
104 *Phtheirospermum* haustorium. Targeted gene-knockouts of *PjIPT1a* by CRISPR/Cas9
105 suppressed parasite-induced cytokinin responses in the host. Similarities to
106 isopentenyltransferases from *Striga* suggest that hemiparasitic Orobanchaceae use common
107 strategies to manipulate host plants.

108 Materials and Methods

109 Plant growth conditions and transformation

110 *Phtheirospermum japonicum* (Okayama, wild-type) seeds were sterilized in 70% ethanol,
111 0.05% SDS for 10 minutes, and then washed with 98% ethanol. For transformation, plants were
112 grown on Gamborg B5 medium (Duchefa) supplemented with 1% sucrose at 25°C under long-
113 day conditions (16 h light). Seven-days-old *Phtheirospermum* seedlings were transformed with
114 *Agrobacterium rhizogenes* AR1193 as previously described (Ishida *et al.*, 2011).
115 Approximately four weeks after transformation, *Phtheirospermum* seedlings with hairy roots
116 were transferred to 0.8% agar containing 300 µg/ml cefotaxime. Two days later, *Arabidopsis*
117 Ws *pARR5:GFP* seedlings grown for one week on MS (Duchefa) plates were aligned next to
118 *Phtheirospermum* hairy roots. One week later, infected plants were transferred to half-strength
119 MS plates and grown for additional 21 days. *Nicotiana benthamiana* plants were grown in soil
120 under long-day conditions at 25°C.

121

122 Phylogenetic analysis

123 IPT amino acid sequences were retrieved from public databases (NCBI), and by blast search
124 using IPT protein sequences as query against published genomes (Table **S1**). CLC Main
125 Workbench Version 8 was used to align protein sequences and to construct a phylogenetic tree
126 based on the UPGMA and Jake-Cantor algorithm with a bootstrap analysis of 1000 replicates.

127

128 Cloning, plasmid design and genotyping

129 We cloned the 2.6 kb upstream sequence of the *PjIPT1a* gene while removing an internal
130 Bpi1site into a Golden Gate vector that was then used to generate 3xVenus-Nuclear
131 Localization Signal (NLS)-based reporter as previously described (Engler *et al.*, 2014; Cui *et*
132 *al.*, 2016). Primer sequences are given in Table **S2**. Open reading frames (ORFs) of *PjIPT1a*
133 and *PjIPT1b* were first cloned into pENTR/D-TOPO entry vector (Thermo Fisher Scientific)
134 to generate GFP fusion constructs using the pGWB5 binary vector (Nakagawa *et al.*, 2007).
135 The putative chloroplast transit peptide was cloned into pART7 using XhoI and ClaI (Thermo
136 Fisher Scientific) and then into pART27 (Gleave, 1992). An empty pGREEN vector was used
137 to express *p35S:GFP* (Hellens *et al.*, 2000). Golden Gate-compatible vectors carrying *PjIPT1a*-
138 specific gRNAs, *Cas9*, and the transformation marker *p35S:DsRED* were assembled as
139 previously described (Nekrasov *et al.*, 2013; Engler *et al.*, 2014). gRNAs were chosen based
140 on their specificity to the intended target. Individual hairy roots were genotyped by amplifying
141 a 1651 bp long amplicon that contained the 954 bp *PjIPT1a* gene. *PjIPT1a* alleles were cloned

142 into pBluescript-II-SK(+) vectors for sequencing. For expression in *E. coli*, ORFs of *PjIPT1a*,
143 *PjIPT1b*, and *GST* were fused with a C-terminal octa-His tag in the pET42 vector (Novagen).
144
145 Expression of proteins in *N. benthamiana* and *E. coli*
146 *Agrobacterium tumefaciens* GV3101 were infiltrated in a 10 mM MES (pH 5.6) and 10 mM
147 $MgCl_2$ buffer into approximately five-week-old *N. benthamiana* leaves, which were imaged
148 two days later. *PjIPT1a-His*, *PjIPT1b-His*, and *GST-His* were expressed in *E. coli* BL21 RIL
149 cells and purified on NiNTA beads (Qiagen), then concentrated and desalted using Vivaspin
150 500 columns (Sartorius).
151
152 Microscopy
153 Hairy roots were imaged in water using a Zeiss Axio Image Z.1 fluorescence microscope.
154 *PjIPT1a* promoter activity was recorded with a Leica TCS SP5 II, the subcellular location of
155 fluorescent proteins with a Zeiss LSM 700 confocal microscope.
156
157 IPT-*in vitro* assays
158 IPT-*in vitro* assays were conducted as previously described (Brugière *et al.*, 2008). In brief, 8
159 µg of purified proteins were incubated with 1 mM DMAPP (Sigma-Aldrich) and 1 mM AMP
160 or ATP for two hours at 30°C in 12.5 mM Tris–HCl (pH 7.5), 37.5 mM KCl, 5 mM $MgCl_2$.
161 The reaction was stopped at 95°C and methanol precipitated. The supernatant was analysed by
162 UHPLC-MS/MS on a 1290 UHPLC system (Agilent) coupled to a Q-Exactive Plus Orbitrap
163 mass spectrometer equipped with a heated electrospray ionization (HESI) source (Thermo
164 Fisher Scientific). Analyte separation was achieved by a Phenomenex Luna Omega Polar C18
165 column. Mobile phase A was 0.2% formic acid in water, and mobile phase B 0.2% formic acid
166 in acetonitrile. The HESI source was operated in positive ion mode, with a capillary voltage of
167 4.2 kV and an ion transfer capillary temperature of 360°C. Mass spectra were acquired in MS
168 mode within the mass range of 150 to 800 m/z at a resolution of 70,000 FWHM using an
169 Automatic Gain Control (AGC) target of 3 × 106 of and 100 ms maximum ion injection time
170 (MIT). Data dependent MS/MS spectra in a mass range of 200 to 2000 m/z were generated for
171 the five most abundant precursor ions with a resolution of 17,500 FWHM using an AGC target
172 of 5 × 104, 64 ms MIT and a stepped collision energy of 15, 30 and 55. Xcalibur software
173 version 4.4.16.14 (Thermo Fisher Scientific) was used for instrument control and data
174 acquisition. Compound Discoverer software 3.2 (Thermo Fischer Scientific) was used for
175 analysing raw instrument data (.raw files) and peak area calculation.

Statistical analysis

The R packages Rmisc, readr, multcompView, ggplot2 and ggpubr were used for statistics (R Core Team, 2020).

180 Results

181 *PjIPT1a* is expressed in intrusive cells of *Phtheirospermum* haustoria

182 CK biosynthesis is tightly regulated by environmental and developmental cues and restricted
183 to distinct tissues and cells. We thus reasoned that CK production in *Phtheirospermum*
184 haustoria requires the haustorium-specific expression of at least one *IPT* gene. We surveyed
185 published *Phtheirospermum* transcriptomes for infection-specific expression of *IPTs* and
186 identified one, hereinafter referred to as *PjIPT1a*, that is upregulated in the course of infection
187 and shows 25-fold higher expression in intrusive cells relative to the rest of the haustorium (Fig.
188 **1b**) (Ogawa *et al.*, 2020). *PjIPT1a* expression increases until day three of the infection and
189 continues at a relatively high level for the later time points (Fig. **1c**) (Kurotani *et al.*, 2020).
190 This expression profile coincides with the induction of CK response markers in parasite and
191 host, which become detectable from 3 - 4 dpi (days post-infection) and remain visible until at
192 least 30 dpi (Spallek *et al.*, 2017). Using a 2.6 kb *PjIPT1a* promoter fragment to drive the
193 expression of a *3xVenus-NLS* reporter, we confirmed the specific expression of the *PjIPT1a*
194 gene in intrusive cells of *Phtheirospermum* haustoria at 4 dpi of *Arabidopsis* roots (Fig. **1d-f**).
195 *PjIPT1a* is thus expressed in cells in close, likely direct, contact to the host vasculature (Fig.
196 **1g-i**).

197

198 *PjIPT1a* encodes a cytosolic IPT with homologs in *Striga hermonthica*

199 To validate the phylogenetic relationship of PjIPT1a to other *Phtheirospermum* IPTs, we
200 compared the amino acid sequences of PjIPTs to known plant IPTs and two agrobacterial IPTs,
201 Tzs and Tmr (Fig. **2a**). PjIPT1a clustered with other plant IPT1s, and was more similar to
202 proteins from the related parasitic species *Striga hermonthica* (Orobanchaceae, Lamiales) and
203 *Streptocarpus rexii* (Gesneriaceae, Lamiales) than to IPTs from more distantly related non-
204 parasitic species such as common hop (*Humulus lupulus*, Cannabaceae, Rosales) and
205 *Arabidopsis thaliana* (Brassicaceae, Brassicales). Two close homologs were detected for
206 PjIPT1a and its *Striga* ortholog ShIPT1a. Like *PjIPT1a*, only *ShIPT1a* is induced upon
207 infections but not *ShIPT1b* (Fig. **S1**).

208

209 Bioinformatics tools predict a chloroplast transit peptide (CTP) in the first 22 amino acids of
210 PjIPT1a; however, at a lower score compared to AtIPT1 and SrIPT1 (Table **S3**). Putative CTPs
211 of PjIPT1a and ShIPT1a are less than half as long as the CTPs predicted for AtIPT1 (71 amino
212 acids) and SrIPT1 (46 amino acids) (Table **S3**; Fig. **S2**). Therefore, we experimentally tested
213 subcellular localization of PjIPT1a and functionality of its CTP. A PjIPT1a-GFP fusion protein

214 transiently expressed in *N. benthamiana* located to cytosol and nucleus (Fig. **2b**), with no
215 apparent difference to the localization of free GFP (Fig. **2e**). Western-blots using anti-GFP
216 antibodies confirmed the integrity of the PjIPT1a-GFP full-length protein (Fig. **S3**). The data
217 thus suggest nuclear-cytoplasmic localization of PjIPT1a.
218
219 Nuclear-cytoplasmic localization is also observed for chloroplast-targeted AtIPT3, when it is
220 post-translationally modified by C-terminal farnesylation (Galichet *et al.*, 2008). To exclude
221 the possibility that post-translational modifications of PjIPT1a outside the putative CTP would
222 affect its localization, we analysed the subcellular targeting of super-folder (sf) GFP fused to
223 the predicted transit peptide (the first 22 amino acids). The localization of PjIPT1a$^{(1-22)}$-sfGFP
224 (Fig. **2c**) was indistinguishable from PjIPT1a-GFP and free GFP (Fig. **2b,e**). The same nuclear-
225 cytoplasmic localization was also observed for PjIPT1b-GFP (Fig. **2d**). The putative CTP signal
226 in *Striga* ShIPT1a is even shorter (11 amino acids) than the apparently non-functional CTP of
227 PjIPT1a (Fig. **S2**; Table **S3**), while no CTP was predicted for ShIPT1b. Therefore, we assume
228 a similar subcellular localization pattern of the homologous ShIPT1a and ShIPT1b proteins.
229
230 PjIPT1a drives CKs responses in host plants
231 Haustorium-derived CKs induce hypertrophy of the host root and can be visualized by a host-
232 expressed cytokinin reporter (*pARR5:GFP*) (Spallek *et al.*, 2017). To address a role for *PjIPT1a*
233 in the production of haustorium-derived CKs, we generated transgenic *Phtheirospermum* roots
234 (hairy roots, HR) that expressed the *Cas9* gene together with two *PjIPT1a*-specific gRNAs (Fig.
235 **3b**). The construct also contained *p35S:dsRED* as a fluorescent marker for identification of
236 transformed roots. HR transformed with *p35S:dsRED* alone (HR1) and hairy roots without the
237 *Cas9/PjIPT1a-gRNA*s + *dsRED* cassette (HR2) served as controls. In contrast to control HRs
238 (HR1-2) that triggered *pARR5:GFP* expression and hypertrophic growth in infected
239 *Arabidopsis* roots, neither *pARR5:GFP* expression nor hypertrophic growth were observed
240 after infection with HRs containing the *Cas9/PjIPT1a-gRNA*s + *dsRED* cassette (HR3-5) (Fig.
241 **3a**). While the *PjIPT1a* locus was successfully PCR-amplified in full length from control HR1-
242 2 (Fig. **3c**), additional smaller bands were observed for *Cas9*-containing HR3-5 (Fig. **3c**).
243 Sequencing *PjIPT1a* amplicons revealed Cas9-induced deletions of the *PjIPT1a* locus ranging
244 from single nucleotides to 1100 bp for HR3-5 (Fig. **3d**). For HR4, we identified three alleles
245 that carried deletions of 40 bp, 893 bp, and 1110 bp in the *PjIPT1a* gene, indicating a chimeric
246 pattern of Cas9-induced mutations in *Phtheirospermum* hairy roots (Fig. **3d**). The presence of
247 Cas9-induced deletions in *PjIPT1a* correlated perfectly with the absence of a

248 *Phtheirospermum*-induced cytokinin response in *Arabidopsis*. We therefore conclude that
249 *PjIPT1a* is an essential component in the CK transfer from parasite to host.
250
251 PjIPT1a and PjIPT1b differ in isopentenyltransferase activity
252 PjIPT1a and ShIPT1a share a unique triple-proline motif close to the nucleotide-binding site
253 that we only found in IPTa isoforms of parasitic Orobanchaceae species (Fig. **S4**). This raised
254 questions regarding their enzymatic activity. We purified His-tagged PjIPT1a and PjIPT1b
255 from *E. coli* and assayed for isoprenylation of AMP and ATP with DMAPP as the isoprenyl
256 donor and His-tagged GST as negative control (Fig. **4**). When AMP was used as substrate, the
257 total amount of isoprenylated products were similar (factor of 1.3) for PjIPT1a-His and
258 PjIPT1b-His (Fig. **4a**). However, with ATP as substrate, the total amount of isoprenylated
259 products was about four times higher for PjIPT1b-His compared to PjIPT1a-His, indicating
260 higher selectivity for ATP over AMP (Fig. **4b**).

261 Discussion

262 Here, we studied parasite-induced CK responses in host plants as an example of a
263 neofunctionalized gene function in the Orobanchaceae species *Phtheirospermum japonicum*
264 and *Striga hermonthica*. We found one *IPT* gene, *PjIPT1a*, to be expressed in *Phtheirospermum*
265 haustoria. Reporter gene analysis revealed spatially restricted activity of the *PjIPT1a* promotor
266 in intrusive cells that are in contact with the host vasculature (Fig. **1g-i**). The proximity to the
267 host vasculature is likely sufficient to transfer cytokinins to the host and to trigger CK responses
268 above the haustorium attachment site (Spíchal, 2012). The parasitic tree *Santalum album* also
269 expresses an IPT1 homolog at a similar stage of infections; however, the exact location of
270 *SaIPT1* expressing cells is not known (Zhang *et al.*, 2015).

271

272 Unlike in *Santalum album* and many other parasitic plants that are not amenable to reverse
273 genetic manipulation, we were able to use CRISPR/Cas9-based loss-of-function analysis to
274 demonstrate that *PjIPT1a* adopted new parasitism-related functions in *Phtheirospermum*.
275 While RNAi-based knock-down approaches have largely been replaced by the CRISPR/Cas9
276 technology, RNAi remained, until now, the only strategy to study parasitic plant genes
277 (Bandaranayake *et al.*, 2010; Alakonya *et al.*, 2012; Wakatake *et al.*, 2020). Here, we report the
278 first successful application of the CRISPR/Cas9 technology for studying loss-of-function
279 phenotypes in parasitic plants. CRISPR/Cas9 efficiently introduced deletions in *PjIPT1a*
280 resulting in the loss of up to 98% of the coding sequence, or in the disruption of its open reading
281 frame. In individual hairy roots, we found more than one, in one instance more than two,
282 mutated alleles of *PjIPT1a*, a result of the occasionally chimeric nature of *Agrobacterium*
283 *rhizogenes*-induced hairy roots (Wakatake *et al.*, 2018). All *Phtheirospermum* roots with non-
284 functional *PjIPT1a* genes failed to induce host CK responses (Fig. **3**).

285

286 Our phylogenetic analysis of *IPTs* showed that the duplication event producing
287 *PjIPT1a/ShIPT1a* and *PjIPT1b/ShIPT1b* occurred in a common non-parasitic ancestor of *P.*
288 *japonicum* and *S. hermonthica* (Fig. **2a**). Surprisingly, *PjIPT1a* and *ShIPT1a*, which were both
289 expressed during infections, were more similar to SrIPT1 from *Streptocarpus rexii* than
290 PjIPT1b and ShIPT1b (Fig. **2a**). The high similarity between parasitism-related and
291 conventional IPTs suggests that neofunctionalization of *PjIPT1a* mainly occurred at the level
292 of its expression profile. Enzymatic constraints may have limited divergence of the gene body
293 and the enzymatic functions of PjIPT1a and b are indeed comparable. However, preference for
294 ATP was reduced in PjIPT1a; its preference for the energetically less costly AMP as

295 isopentenyl donor may reflect an adaptation to the resource-limited parasitic lifestyle that is
296 induced under nutrient-deficient conditions (Spallek *et al.*, 2017). A notable exception to the
297 similarity of PjIPT1a and ShIPT1a to SrIPT1 is a characteristic triple-proline-motif that is only
298 found in parasitism-related IPTs (Fig. **S4**).
299
300 Another unexpected feature of PjIPT1a is its nuclear-cytoplasmic localization (Fig. **2b,c**),
301 which it shares with PjIPT1b (Fig. **2d**) and likely also with ShIPT1a and ShIPT1b (Table **S3**).
302 *Arabidopsis* AtIPT1 and AtIPT3 feature functional N-terminal CTPs (Kasahara *et al.*, 2004).
303 However, while AtIPT1 is located in plastids, AtIPT3 is dually targeted, either to the chloroplast,
304 or to the nucleus/cytoplasm in a farnesylation-dependent manner (Galichet *et al.*, 2008). We
305 can exclude a similar mechanism for PjIPT1a, as its predicted CTP appeared to be non-
306 functional, as it was insufficient for targeting GFP to plastids (Fig. **2c**). The relevance of the
307 nuclear-cytoplasmic localization is not clear, but given that it is shared between IPTs that are
308 upregulated during infection and others that are not, a functional link to parasitism seems
309 unlikely.
310
311 In conclusion, targeted knock-outs of *PjIPT1a* and its expression in intrusive cells of the
312 haustorium revealed an essential role of PjIPT1a for *Phtheirospermum*-induced CK responses
313 in *Arabidopsis.* The *PjIPT1a* gene likely originated from a non-parasitic ancestral gene through
314 gene duplication followed by neofunctionalization. PjIPT1a has homologs in other parasitic
315 plants. Targeting of neofunctionalized genes in parasitic plants may allow for specific control
316 of parasitic weeds leaving host plants unharmed.

Acknowledgements

This work supported by the German Research Foundation (DFG, 424122841) to T.S and MEXT KAKENHI JP20H05909 to S.Y. and K.S. The authors thank Ursula Glück-Behrens and Ute Bertsche for technical support.

Author Contribution

T.S., A.S., and K.S supervised the research. A.G. and I.B. analysed the subcellular location of proteins, purified IPTs from *E. coli* and conducted the *in vitro* assays. J.P. measured the IPT *in vitro* assays compounds by HPLC-MS/MS. T.S. performed the remaining experiments. A.S., P.S., and T.S. analysed data. Y.S. and K.S. provided crucial non-published data. T.S. and A.S. wrote the paper.

Data Availability

Table **S1** contains accession numbers of genes and proteins used in this study. Gene sequences for *PjIPT1a* and *PjIPT1b* were deposited in the NCBI Gene Bank under the accession numbers MZ441091 and MZ441090, respectively. Previously published sequencing data is available from at the Dryad database (https://doi.org/10.5061/dryad.vt4b8gtpt) and at the National Center for Biotechnology Information, NCBI, (https://www.ncbi.nlm.nih.gov/sra/DRX219041[accn] for *Phtheirospermum japonicum* and https://doi.org/10.5061/dryad.53t3574 for *Striga hermonthica*).

References

Akiyoshi DE, Klee H, Amasino RM, Nester EW, Gordon MP. 1984. T-DNA of *Agrobacterium tumefaciens* encodes an enzyme of cytokinin biosynthesis. *Proceedings of the National Academy of Sciences*, *USA* **81**: 5994–5998.

Alakonya A, Kumar R, Koenig D, Kimura S, Townsley B, Runo S, Garces HM, Kang J, Yanez A, David-Schwartz R, *et al.* 2012. Interspecific RNA interference of *SHOOT MERISTEMLESS*-like disrupts *Cuscuta pentagona* plant parasitism. *Plant Cell* **24:** 3153–3166.

Bandaranayake PCG, Filappova T, Tomilov A, Tomilova NB, Jamison-McClung D, Ngo Q, Inoue K, Yoder JI. 2010. A single-electron reducing quinone oxidoreductase is necessary to induce haustorium development in the root parasitic plant *Triphysaria*. *Plant Cell* **22:** 1404–1419.

350 **Brugière N, Humbert S, Rizzo N, Bohn J, Habben JE. 2008.** A member of the maize
351 isopentenyl transferase gene family, *Zea mays isopentenyl transferase 2* (*ZmIPT2*), encodes a
352 cytokinin biosynthetic enzyme expressed during kernel development. *Plant Molecular Biology*
353 **67:** 215–229.
354 **Brun G, Spallek T, Simier P, Delavault P. 2020.** Molecular actors of seed germination and
355 haustoriogenesis in parasitic weeds. *Plant Physiology* **185:** 1270-1281.
356 **Brundrett MC, Tedersoo L. 2018.** Evolutionary history of mycorrhizal symbioses and global
357 host plant diversity. *New Phytologist* **220:** 1108–1115.
358 **Clarke CR, Timko MP, Yoder JI, Axtell MJ, Westwood JH. 2019.** Molecular dialog
359 between parasitic plants and their hosts. *Annual Review of Phytopathology* **57:** 279–299.
360 **Cui S, Wakatake T, Hashimoto K, Saucet SB, Toyooka K, Yoshida S, Shirasu K. 2016.**
361 Haustorial hairs are specialized root hairs that support parasitism in the facultative parasitic
362 plant *Phtheirospermum japonicum*. *Plant Physiology* **170:** 1492–1503.
363 **Engler C, Youles M, Gruetzner R, Ehnert TM, Werner S, Jones JDG, Patron NJ,**
364 **Marillonnet S. 2014.** A Golden Gate modular cloning toolbox for plants. *ACS Synthetic*
365 *Biology* **3:** 839–843.
366 **Furuhashi T, Kojima M, Sakakibara H, Fukushima A, Hirai MY, Furuhashi K. 2013.**
367 Morphological and plant hormonal changes during parasitization by *Cuscuta japonica* on
368 *Momordica charantia*. *Journal of Plant Interactions* **9:** 220–232.
369 **Galichet A, Hoyerová K, Kamínek M, Gruissem W. 2008.** Farnesylation directs AtIPT3
370 subcellular localization and modulates cytokinin biosynthesis in *Arabidopsis*. *Plant Physiology*
371 **146:** 1155–1164.
372 **Gleave AP. 1992.** A versatile binary vector system with a T-DNA organisational structure
373 conducive to efficient integration of cloned DNA into the plant genome. *Plant Molecular*
374 *Biology* **20:** 1203–1207.
375 **Heide-Jorgensen H. 2008.** *Parasitic Flowering Plants.* Leiden: Brill Academic Publishers.
376 **Heinemeyer W, Buchmann I, Tonge DW, Windass JD, Alt-Moerbe J, Weiler EW, Botz T,**
377 **Schröder J. 1987.** Two *Agrobacterium tumefaciens* genes for cytokinin biosynthesis: Ti
378 plasmid-coded isopentenyltransferases adapted for function in prokaryotic or eukaryotic cells.
379 *Molecular and General Genetics* **210:** 156–164.
380 **Hellens RP, Edwards E a, Leyland NR, Bean S, Mullineaux PM. 2000.** pGreen: a versatile
381 and flexible binary Ti vector for *Agrobacterium*-mediated plant transformation. *Plant*
382 *Molecular Biology* **42:** 819–832.

383 **Ishida JK, Yoshida S, Ito M, Namba S, Shirasu K. 2011.** *Agrobacterium rhizogenes-*
384 mediated transformation of the parasitic plant *Phtheirospermum japonicum*. *PloS one* **6:**
385 e25802.
386 **Kakimoto T. 2001.** Identification of plant cytokinin biosynthetic enzymes as dimethylallyl
387 diphosphate:ATP/ADP isopentenyltransferases. *Plant and Cell Physiology* **42:** 677–685.
388 **Kasahara H, Takei K, Ueda N, Hishiyama S, Yamaya T, Kamiya Y, Yamaguchi S,**
389 **Sakakibara H. 2004.** Distinct isoprenoid origins of cis- and trans-zeatin biosyntheses in
390 *Arabidopsis*. *Journal of Biological Chemistry* **279:** 14049–14054.
391 **Kieber JJ, Schaller GE. 2014.** Cytokinins. *The Arabidopsis Book* **12:** e0168.
392 **Kokla A, Melnyk CW. 2018.** Developing a thief: Haustoria formation in parasitic plants.
393 *Developmental Biology* **442:** 53–59.
394 **Kurotani K, Wakatake T, Ichihashi Y, Okayasu K, Sawai Y, Ogawa S, Suzuki T, Shirasu**
395 **K, Notaguchi M. 2020.** Host-parasite tissue adhesion by a secreted type of β-1,4-glucanase in
396 the parasitic plant *Phtheirospermum japonicum*. *Communications Biology* **3:** 407.
397 **Nakagawa T, Kurose T, Hino T, Tanaka K, Kawamukai M, Niwa Y, Toyooka K,**
398 **Matsuoka K, Jinbo T, Kimura T. 2007.** Development of series of gateway binary vectors,
399 pGWBs, for realizing efficient construction of fusion genes for plant transformation. *Journal*
400 *of Bioscience and Bioengineering* **104:** 34–41.
401 **Nekrasov V, Staskawicz B, Weigel D, Jones JDG, Kamoun S. 2013.** Targeted mutagenesis
402 in the model plant *Nicotiana benthamiana* using Cas9 RNA-guided endonuclease. *Nature*
403 *Biotechnology* **31:** 691–693.
404 **Nickrent DL. 2020.** Parasitic angiosperms: How often and how many? *TAXON* **69:** 5–27.
405 **Ogawa S, Wakatake T, Spallek T, Ishida JK, Sano R, Kurata T, Demura T, Yoshida S,**
406 **Ichihashi Y, Schaller A, Shirasu K., 2020.** Subtilase activity in intrusive cells mediates
407 haustorium maturation in parasitic plants. *Plant Physiology* **185:** 1381-1394.
408 **R Core Team 2020.** R: A language and environment for statistical computing. R Foundation
409 for Statistical Computing, Vienna, Austria.
410 **Sakakibara H. 2006.** Cytokinins: activity, biosynthesis, and translocation. *Annual Review of*
411 *Plant Biology* **57:** 431–49.
412 **Spallek T, Melnyk CW, Wakatake T, Zhang J, Sakamoto Y, Kiba T, Yoshida S,**
413 **Matsunaga S, Sakakibara H, Shirasu K. 2017.** Interspecies hormonal control of host root
414 morphology by parasitic plants. *Proceedings of the National Academy of Sciences*, *USA* **114:**
415 5283–5288.

416 **Spíchal L. 2012.** Cytokinins - Recent news and views of evolutionally old molecules.
417 *Functional Plant Biology* **39:** 267–284.
418 **Sun G, Xu Y, Liu H, Sun T, Zhang J, Hettenhausen C, Shen G, Qi J, Qin Y, Li J, et al.**
419 **2018.** Large-scale gene losses underlie the genome evolution of parasitic plant *Cuscuta*
420 *australis*. *Nature Communications* **9:** 2683.
421 **Vogel A, Schwacke R, Denton AK, Fischer K, Bolger A, Marie E, Gundlach H, Mayer**
422 **KFX, Weiss-Schneeweiss H, Eva M, et al. 2018.** Footprints of parasitism in the genome of
423 the parasitic flowering plant *Cuscuta campestris*. *Nature Communications* **9:** 2515.
424 **Wakatake T, Ogawa S, Yoshida S, Shirasu K. 2020.** An auxin transport network underlies
425 xylem bridge formation between the hemi-parasitic plant *Phtheirospermum japonicum* and host
426 *Arabidopsis*. *Development* **147:** dev187781.
427 **Wakatake T, Yoshida S, Shirasu K. 2018.** Induced cell fate transitions at multiple cell layers
428 configure haustorium development in parasitic plants. *Development* **145:** dev164848.
429 **Yang Z, Wafula EK, Honaas LA, Zhang H, Das M, Fernandez-Aparicio M, Huang K,**
430 **Bandaranayake PCG, Wu B, Der JP, et al. 2015.** Comparative transcriptome analyses reveal
431 core parasitism genes and suggest gene duplication and repurposing as sources of structural
432 novelty. *Molecular Biology and Evolution* **32:** 767–790.
433 **Yoshida S, Cui S, Ichihashi Y, Shirasu K. 2016.** The Haustorium, a specialized invasive
434 organ in parasitic plants. *Annual Review of Plant Biology* **67:** 643–667.
435 **Yoshida S, Kim S, Wafula EK, Tanskanen J, Kim Y-M, Honaas L, Yang Z, Spallek T,**
436 **Conn CE, Ichihashi Y, et al. 2019.** Genome sequence of *Striga asiatica* provides insight into
437 the evolution of plant parasitism. *Current Biology* **29:** 3041-3052.
438 **Zhang X, Berkowitz O, Teixeira da Silva JA, Zhang M, Ma G, Whelan J, Duan J. 2015.**
439 RNA-Seq analysis identifies key genes associated with haustorial development in the root
440 hemiparasite *Santalum album*. *Frontiers in Plant Science* **6:** 661.
441 **Zhang X, Teixeira da Silva JA, Duan J, Deng R, Xu X, Ma G. 2012.** Endogenous hormone
442 levels and anatomical characters of haustoria in *Santalum album* L. seedlings before and after
443 attachment to the host. *Journal of Plant Physiology* **169:** 859–866.

444 Figure legends

445

446 **Figure 1:** ***PjIPT1a* is specifically expressed in intrusive cells.** (a) Prenylation of ATP,
447 ADP and AMP by isopentenyltransferases (IPT) with di-methylallyl pyrophosphate (DMAPP)
448 to isopentenyladenosine-5'-triphosphate (IPRTP), isopentenyladenosine-5'-diphosphate
449 (IPRDP) and isopentenyladenosine-5'-monophosphate (IPRMP) is the first step of cytokinin
450 (CK) biosynthesis. (b) RNA-Sequencing data (originally published in Ogawa et al., 2020)
451 shows increased expression of *PjIPT1a* in intrusive cells of *Phtheirospermum* haustoria 5 days
452 post-infection (dpi) of rice roots (*Oryza sativa*, *Os*). (c) Upregulation of *PjIPT1a* expression
453 during infection of *Arabidopsis* (*At*) roots peaks with 61 CPM (counts per million mapped
454 reads) at 3 dpi (RNA-Sequencing data from Kurotani et al., 2020). (b, c) Colour gradients
455 (white-yellow-red) relate to *PjIPT1a* expression in indicated sampling areas. Haustoria
456 diagrams are based on haustoria outlines presented in Brun et al. 2020. (d - i) Confocal images
457 show a *Phtheirospermum* (*Pj*) haustorium expressing *pIPT1:3xVenus-NLS* during infection of
458 *Arabidopsis* (*At*) at 4 dpi. Merged yellow channel for Venus detection and bright-field is
459 depicted in (d), individual Venus and bright-field channels in (e) and (f), respectively. Zoomed-
460 in scans shown in g - i correspond to the region marked by dotted lines in (d – f). Intrusive cells
461 are indicated with white arrows. Scale bars = 100 µm.

462

463 **Figure 2:** ***PjIPT1a* and its closest homolog are nuclear-cytoplasmic IPTs.** Phylogenetic
464 analysis (UPGMA) based on the amino acid sequences of prokaryotic (*Agrobacterium*) and
465 plant IPTs positions IPT1a within a cluster of plant IPT1s and closest to the *Striga* ShIPT1a
466 protein. Bootstrap values are shown as percentage of 1000 repetitions. (b-e) PjIPT1a and
467 PjIPT1b located in the cytoplasm and nucleus when expressed in *N. benthamiana*. The
468 subcellular localization pattern of the full-length PjIPT1a-GFP (b) and PjIPT1b-GFP (d)
469 fusions matched the pattern observed for PjIPT1a$^{(1-22)}$-sfGFP (c) and free GFP (e). Scale bar =
470 50 µm.

471

472 **Figure 3:** ***PjIPT1a* drives host CK responses at the haustorium.** (a) Control (con.)
473 haustoria of hairy roots (HR) without the *Cas9/PjIPT1a-gRNA*s cassette (HR1, 2) induced the
474 expression of host CK-response reporter *pARR5:GFP* and hypertrophic growth (arrows)
475 whereas haustoria with the *Cas9/PjIPT1a-gRNA*s cassette (HR3-5) did not. Images were taken
476 at 28 dpi, scale bars = 100 µm. (b) Schematic representation of the *PjIPT1a* gene flanked by
477 the 5' and 3' extensions that were amplified in (c). The red colour highlights the target

478 sequences of the guide RNAs. (c) PCR amplicons of the *PjIPT1a* (upper panel) and
479 the *Cas9* genes (lower panel) in *Phtheirospermum* hairy roots were separated on agarose gels
480 and stained with Gel Red. (d) Sequencing results of amplicons shown in c with PAM sequences
481 depicted in orange, the start codon in bold font and Cas9-induced mutations in red show
482 different *PjIPT1a* alleles isolated from indicated hairy roots.
483
484 **Figure 4: PjIPT1a and PjIPT1b are isopentyltransferases.** Plots show average +/- SD
485 (n = 3 – 6) peak areas of extracted-ion chromatograms of individual and cumulative (sum)
486 quantifications of isoprenylated derivatives that were detected in reaction mixtures containing
487 DMAPP, equal amounts of *E. coli* purified GST-His, PjIPT1a-His or PjIPT1b-His, and (a)
488 AMP or (b) ATP as isoprenoid acceptors. Different lower-case letters indicate significant
489 differences according to Tukey HSD with $P < 0.05$. ND, not detected

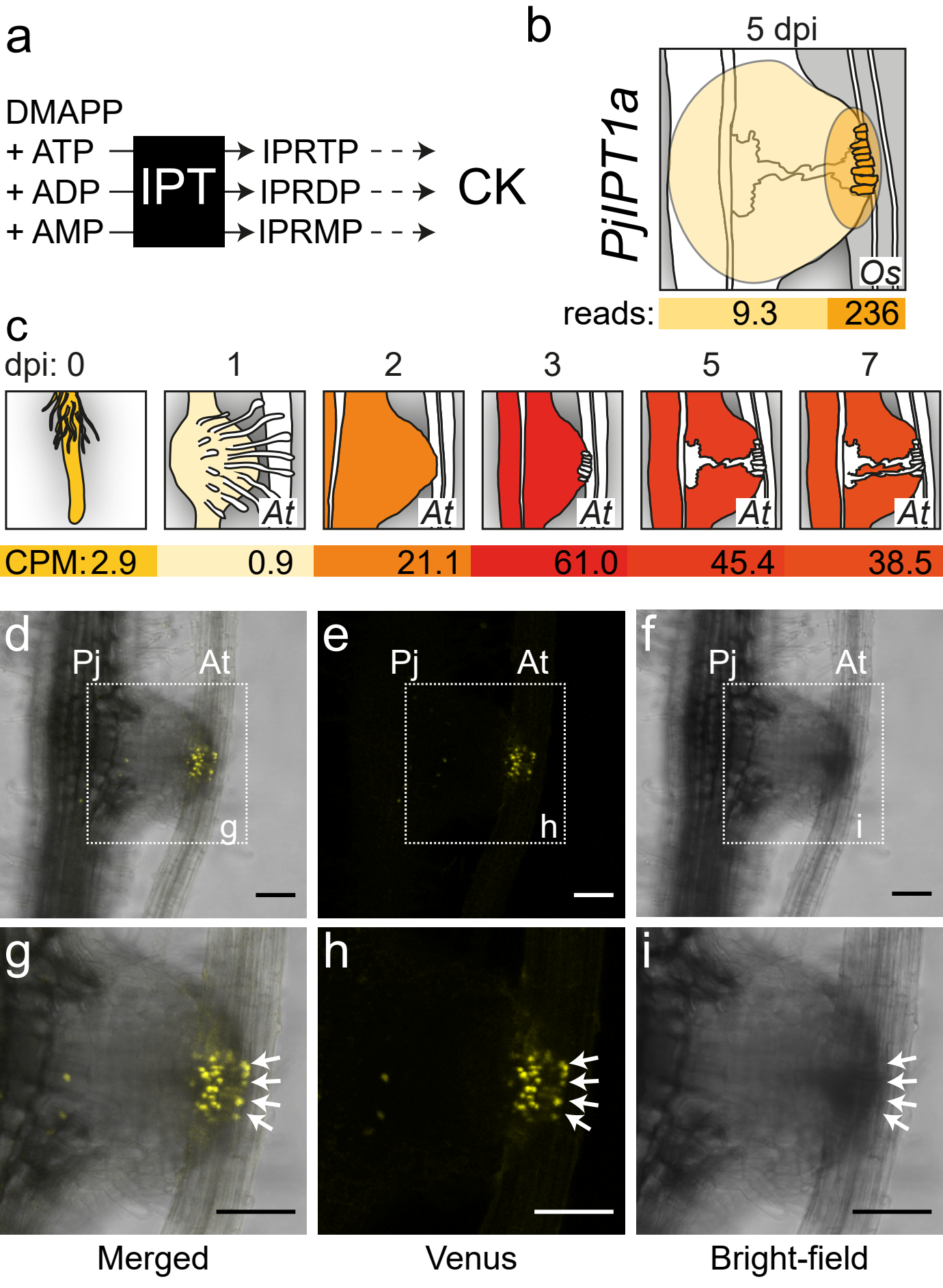
a
DMAPP
+ ATP
+ ADP
+ AMP
IPT
IPRTP
IPRDP
IPRMP
CK
b
5 dpi
PjIPT1a
Os
reads:
9.3
236
c
dpi: 0
1
2
3
5
7
At
CPM:2.9
0.9
21.1
61.0
45.4
38.5
d
e
f
Pj
At
g
h
i
Merged
Venus
Bright-field

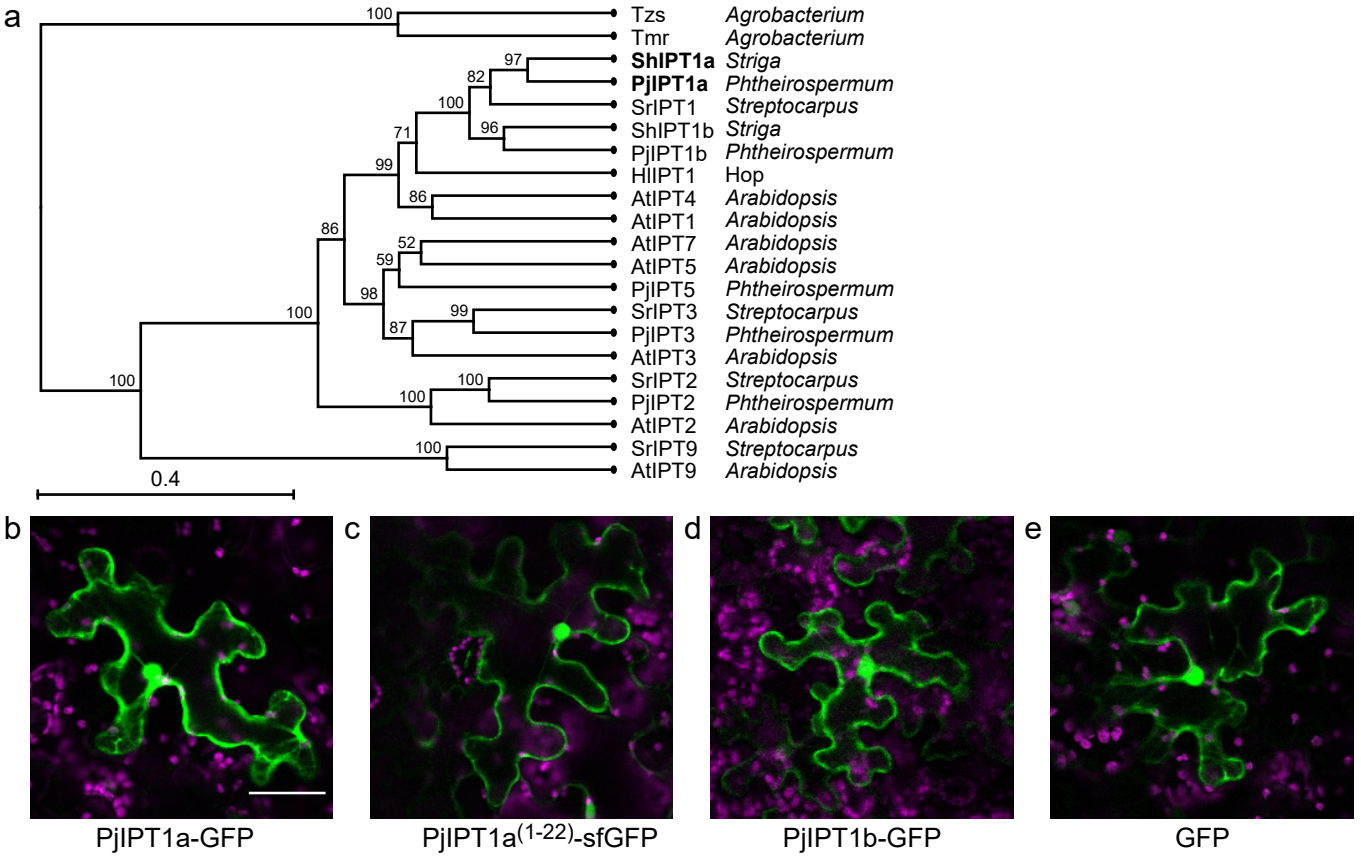
a
Tzs Agrobacterium
Tmr Agrobacterium
ShIPT1a Striga
PjIPT1a Phtheirospermum
SrIPT1 Streptocarpus
ShIPT1b Striga
PjIPT1b Phtheirospermum
HlIPT1 Hop
AtIPT4 Arabidopsis
AtIPT1 Arabidopsis
AtIPT7 Arabidopsis
AtIPT5 Arabidopsis
PjIPT5 Phtheirospermum
SrIPT3 Streptocarpus
PjIPT3 Phtheirospermum
AtIPT3 Arabidopsis
SrIPT2 Streptocarpus
PjIPT2 Phtheirospermum
AtIPT2 Arabidopsis
SrIPT9 Streptocarpus
AtIPT9 Arabidopsis
0.4
b
PjIPT1a-GFP
c
PjIPT1a(1-22)-sfGFP
d
PjIPT1b-GFP
e
GFP

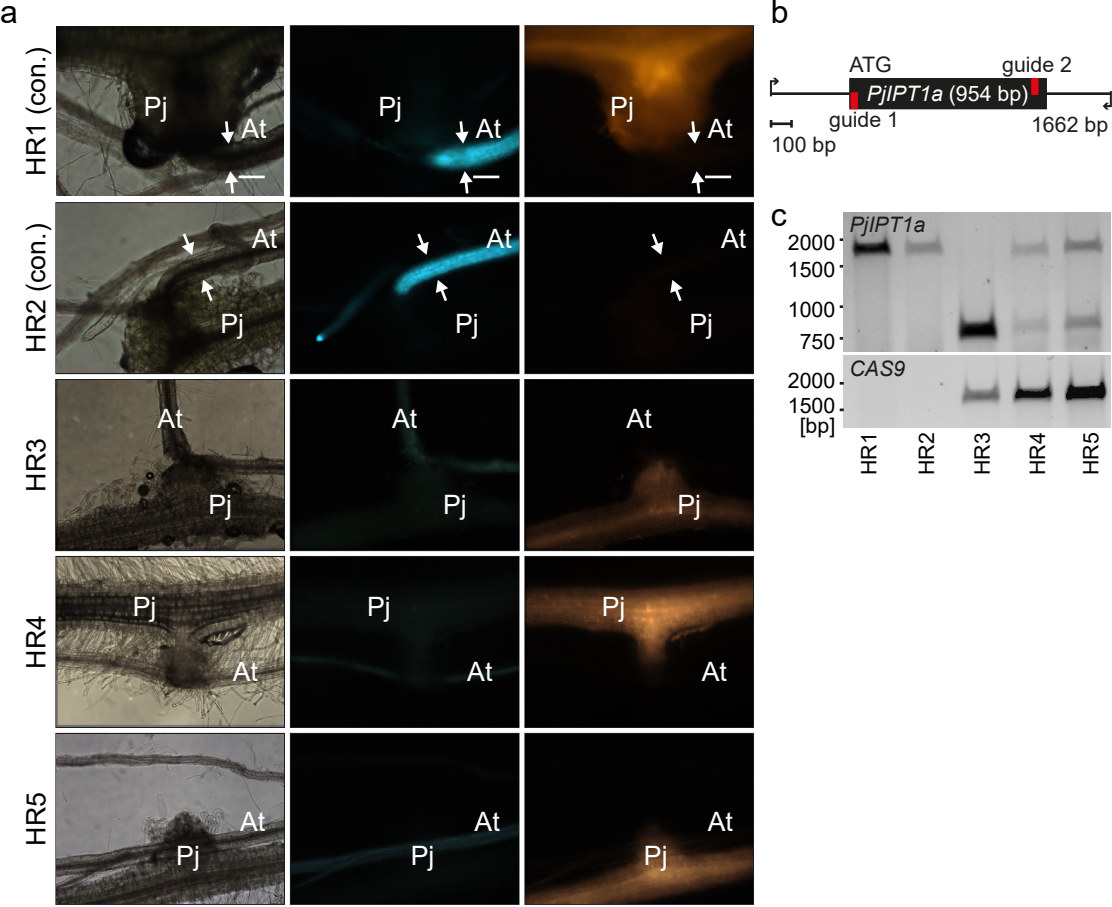

d

HR1 + HR2	GGGCCCCCATGGCGTCCACCACCACCG	AGAGGGAGGTGGTGGAACCAAGCG (Wt)
	GGGCCCCCATGGCGTCCACCACCACCG	AGAGGGAGGTGGTGGAACCAAGCG (Wt)
HR3	GGGCCCCCA----------	----------AGCG (-917)
	GGGCCCCCATGGCGTCCACCACCACCG	AGAGGGAGG-GGTGGAACCAAGCG (-1)
HR4	GGGCCCCCATGGCGTCCACCACCACCG	----------TGGAACCAAGCG (-40)
	GGGCCCCCATGGCGTCCACCA------	---------TGGTGGAACCAAGCG (-893)
	GGGCCCCCATGGCGTCCACCA------	----------(-1110)
HR5	GGGCCCCCATGGCGTCCACCAC----G	AGAGGGAG-TGGTGGAACCAAGCG (-4/-1)
	GGGCCCCCATGGCGTCCACCA------	---------TGGTGGAACCAAGCG (-894)

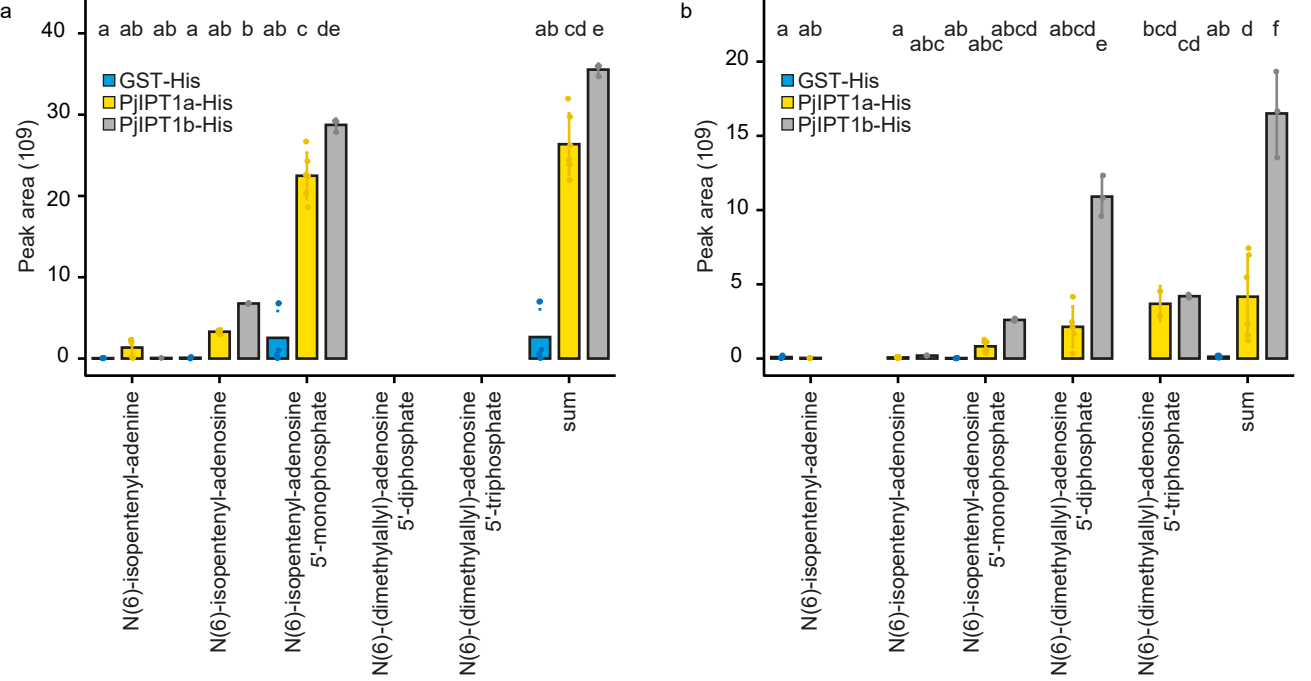
a
b
Peak area (10⁹)
GST-His
PjIPT1a-His
PjIPT1b-His
a ab ab a ab b ab c de ab cd e
a ab a abc ab abc abcd abcd e bcd cd ab d f
N(6)-isopentenyl-adenine
N(6)-isopentenyl-adenosine
N(6)-isopentenyl-adenosine 5'-monophosphate
N(6)-(dimethylallyl)-adenosine 5'-diphosphate
N(6)-(dimethylallyl)-adenosine 5'-triphosphate
sum